Available online at www.sciencedirect.com

SciVerse ScienceDirect

Ceramics International 39 (2013) 7367–7378

CERAMICS INTERNATIONAL

www.elsevier.com/locate/ceramint

Effect of preparation parameters on the morphologically induced photocatalytic activities of hierarchical zinc oxide nanostructures

Parag V. Adhyapak*, Satish P. Meshram, Vijaykumar Tomar, Dinesh P. Amalnerkar, Imtiaz S. Mulla*

Centre for Materials for Electronics Technology, Panchawati, Pashan Road, Pune 411008, India

Received 3 February 2013; received in revised form 22 February 2013; accepted 23 February 2013
Available online 6 March 2013

Abstract

Hierarchical zinc oxide nanostructures were successfully synthesized by facile hydrothermal and sonochemical routes using citrate and PEG as structure directing agents. The effect of precursor concentration and preparation methods on the formation of typical morphology was systematically studied under hydrothermal and sonochemical conditions. Different concentrations of zinc acetate, sodium citrate and NaOH under hydrothermal and sonochemical methods generate different hierarchical structures such as flower-like, cabbage-like, and ellipsoidal ball-like morphologies, depending on the preparation conditions. The as-prepared ZnO samples were characterized by X-ray diffraction (XRD), field emission scanning electron microscopy (FE-SEM), transmission election microscopy (TEM), photoluminescence (PL) spectroscopy, Fourier transform infrared spectroscopy (FTIR) and particle size distribution (PSD) analysis. Catalytic activities of the as-prepared samples were studied by photodegradation of Methylene blue.

Keywords: Zinc oxide; Hydrothermal; Sonochemical; Methylene blue; Photocatalytic activity

1. Introduction

Zinc oxide (ZnO) is an important functional oxide semiconductor with a direct wide band gap (3.37 eV), deep violet/borderline ultraviolet (UV)) and a large exciton binding energy (60 meV). It is a highly preferred multi-tasking metal oxide having a vast list of attractive properties [1]. Due to its unique optical and electrical properties [2,3], it is regarded as a potential material in optoelectronic applications operating in the visible and near ultraviolet spectral regions. The areas in which it is used include UV light-emitting diodes [1,4,5], nanolasers [6], gas sensors [7], highly-efficient green phosphors [8], photo-catalysts and photovoltaic devices [9,10], field-effect transistors [11], chemical sensors [12], transparent conductors and varistors [13,14]. Also, it possesses excellent thermal and chemical stability, a large piezoelectric coefficient, and an easily modifiable electrical conductivity.

The tremendous interest in ZnO is due to its unique ability of possessing structure-dependent properties [15]. Properties like electrical and thermal transport, in addition to optical and mechanical properties, could be varied with respect to particle size, shape, morphology, orientation and aspect ratio. Hence, morphology and dimensionality-controlled growth of zinc oxide has become a challenging topic lately to design novel functional devices. Accordingly, many types of ZnO nanostructures, such as nanowires, nanorod arrays, nanocombs, nanobelts, nanorings, nanocables, and other nanostructures have been synthesized by various processes, such as thermal evaporation deposition, template-mediated growth, metal-organic vapor phase epitaxy and the carbothermic method [16–21]. However, most of the synthesis techniques require high temperature, vacuum, or complicated controlling processes. Therefore, it is of great importance and necessity to develop a technique operating at mild reaction conditions. Hydrothermal and sonochemical methods have been proven to be

*Corresponding authors. Tel.: +91 020 258 997 73; fax: +91 020 2589 8180.
E-mail addresses: adhyapakp@yahoo.com (P.V. Adhyapak), is.mulla@ncl.res.in, ismulla2001@gmail.com (I.S. Mulla).

0272-8842/$ - see front matter © 2013 Elsevier Ltd and Techna Group S.r.l. All rights reserved.
http://dx.doi.org/10.1016/j.ceramint.2013.02.076

a versatile approach for preparation of ZnO due the convenience and simplicity in their operation.

More recently, ZnO architectures with different morphologies synthesized via template-assisted hydrothermal or sonochemical methods have been greatly highlighted [22,23]. Yin et al. employed water-soluble biopolymer sodium carboxymethyl cellulose (CMC)-assisted hydrothermal method for synthesis of hierarchical ZnO nanorod-assembled hollow superstructures for catalysis and photoluminescence applications [24]. Wu et al. have developed a facile amino acid histidine assisted hydrothermal route to synthesize ZnO hierarchical architectures, including prism-like and flower-like structures and hollow microspheres, and they exhibit different photocatalytic activities [25]. Mishra et al. have reported synthesis and growth of flower-like ZnO nanostructures using starch assisted sonochemical method [26]. Moreover, in this context, several different soft templates/capping agents such as ethylene diamine [27], water-soluble diblock copolymers [28] and surfactants [29] have been successfully used to tune the size and shape of ZnO nanostructures. Vaishampayan et al. have reported a low temperature (4 °C) synthesis of crystalline flower-like ZnO by using an aminolytic reaction at the air-liquid interface in an aqueous media at an alkaline pH. They have further reported that nanobelts overlap systematically to form petals of the flower-like structure. The photodegradation of methylene blue over the flower-like ZnO catalyst was observed which was attributed to sub-bands formed due to surface defects facilitating separation of charge carriers which increases their lifetime [30]. In most of these methods of preparing hierarchical ZnO nanostructures, the externally added surfactants or capping agents were adsorbed preferentially on some crystal planes of the growing particles that ultimately alter the growth kinetics and relative stability of the crystal faces and hence either promote or inhibit crystal growth in some particular crystal planes, resulting in the formation of anisotropic ZnO nanostructures. These studies showed high morphology controllability of ZnO; however, most organic additives used in these methods were expensive long chain molecules. Polyethylene glycol (PEG), an inexpensive non-ionic surfactant has been used to assist the formation of metal oxides in previous researches [31,32]. PEG with uniform and ordered chain structure is easily adsorbed at the surface of metal oxide colloid. When this occurs, the surface activity of colloid would greatly decrease. From the view of kinetics of colloid growth, if the colloid adsorbs the polymer on some area of its surface, the growth rate of colloid in some certain direction would be confined. Therefore, the addition of PEG in the metal oxide colloids will modify the growth kinetics of colloid, which finally leads to anisotropic growth of crystals [33–35].

In this article, we report a facile synthesis of ZnO with different morphologies via hydrothermal and sonochemical processes with PEG, trisodium citrate and zinc acetate as the Zn^{2+} source. Citric acid is a weak organic acid and often used as chelating agent. Herein, PEG was introduced as an assembling and structure directing agent along with sodium citrate for controlled synthesis of ZnO architectures assisted by hydrothermal and sonochemical processes. We have studied the effect of precursor concentration and the effect of preparation methods on the morphology of the resulting ZnO nanostructures. Different experimental conditions plays a vital role during the formation of hierarchical morphologies of ZnO such as flower-like, cabbage-like, ellipsoidal ball-like and flake-like structures. The as-synthesized ZnO samples were investigated in terms of their morphology, crystallinity, growth mechanism and photocatalytic efficiency towards degradation of methylene blue dye.

2. Experimental

2.1. Materials

Zinc acetate dihydrate ($Zn(CH_3COO)_2 \cdot 2\,H_2O$) and sodium hydroxide (NaOH) were purchased from Merck (India). Trisodium citrate dihydrate and PEG-400 was purchased from SRL (India). Double distilled water was used to prepare solutions throughout all experiments.

2.2. Preparation of hierarchical ZnO nanostructures

In a typical preparation method, 50 mL of 0.1 M aqueous $Zn(CH_3COO)_2 \cdot 2\,H_2O$ and 50 mL of 0.34 M aqueous Sodium citrate solutions were added to 30 mL PEG-400 under magnetic stirring. Then, 20 mL of 1.8 mM aqueous NaOH solution was added drop-wise to the above emulsion. The resulting mixture was magnetically stirred for 30 min at room temperature and then treated under hydrothermal and sonochemical conditions. For hydrothermal treatment, the reaction mixture was transferred into a Teflon-lined stainless-steel autoclave with a capacity of 200 mL, sealed and maintained at 120 °C for 12 h. The autoclave subsequently cooled to room temperature naturally. The obtained precipitate was centrifuged at 5000 rpm for 15 min, washed with distilled water several times and finally dried at 60 °C in air for 8 h.

Similarly, for sonochemical treatment, the magnetically stirred reaction mixture was irradiated with ultrasound probe (Sonics Vibra cell, USA) for 2 h (with 5 s pulse ON and 1 s pulse OFF at amplitude of 30%). The obtained precipitate was then centrifuged, washed and dried as earlier.

In order to investigate the influence of precursor concentration and the preparation method on the morphology of ZnO nanostructures, a series of experiments were carried out by varying the concentration of the reactants by keeping the quantity of PEG constant. More specifically, the molarity of zinc salt, trisodium citrate and NaOH was decreased systematically by keeping the quantity of PEG and water same. The various preparation conditions and the resultant morphologies are summarized in Table 1.

Table 1
Reaction parameters for the preparation of ZnO nanostructures and their characterization data.

Sample code	[Zinc acetate] (M)	[Sodium citrate] (M)	[NaOH]	PEG-400 (mL)	Yield (%)	Morphology obtained	Size (μm)	$R_{(002)/(101)}$
Hydrothermal method[a]								
HT-1	0.1	0.34	1.8×10^{-3}	30	98	Flower-like	1–3	0.86
HT-2	0.05	0.17	9.3×10^{-4}	30	97	Flower-like	3–5	0.81
HT-3	0.03	0.11	6.2×10^{-4}	30	98	Flower-like	1.5	0.79
Sonochemical method[b]								
SC-1	0.1	0.34	1.8×10^{-3}	30	98	Cabbage-like	1.6	0.88
SC-2	0.05	0.17	9.3×10^{-4}	30	96	Not defined	2–5	0.82
SC-3	0.03	0.11	6.2×10^{-4}	30	98	Ellipsoidal	3–5	0.81

[a]Reaction temperature = 120 °C, reaction time = 12 h (hydrothermal method).
[b]Time = 2 h (with 5 s pulse ON and 1 s pulse OFF at amplitude of 30% (sonochemical method).

2.3. Characterization

The phase identification of the ZnO powders was obtained by X-ray diffraction (XRD) recorded using a Rigaku Miniflex X-ray diffractometer with CuKR irradiation at $\lambda = 1.5406$ Å. The surface morphology of prepared samples was investigated by Field Emitting Scanning Electron Microscopy (FE-SEM) using a JEOL-JSM Model 6700F field-emission scanning electron microscope. The room-temperature photoluminescence spectra of aqueous suspension were recorded on an F-2500 Fluorescence spectrophotometer. For PL measurement, the samples' water suspensions were excited at a wavelength of 340 nm. The particle size distribution measurements of the as-prepared samples was done by dynamic light scattering technique via laser input energy of 632 nm using a PSS-NICOMP particle sizing system, Santa Barbara, California, USA. UV–visible absorption spectra of an aqueous suspension were recorded on a JASCO V-570 spectrophotometer by transferring an appropriate volume of ZnO suspension to quartz cuvette. The spectral changes in concentration of MB during photocatalytic degradation were also studied using the same spectrophotometer. FTIR spectra of as-prepared purified powdered samples were recorded using KBr pellets on a Perkin Elmer 1090 spectrometer.

2.4. Photochemical experiments

The photocatalytic activities of the as-prepared samples were evaluated by measuring the degradation of Methylene Blue (MB) in aqueous solutions under sunlight irradiation. All the experiments of photodegradation reaction were carried out in a 100 mL beaker with a diameter of 6.5 cm. For each experiment, 50 mg of photocatalyst was dispersed in 100 mL of 100 ppm of the MB aqueous solution. Prior to sunlight irradiation, the suspensions were magnetically stirred in the dark for 30 min to ensure the adsorption/desorption equilibrium of MB aqueous solution with the photocatalyst. Five milli litres of the aliquots were sampled at regular intervals of 15 min and analyzed by recording variations in the absorption band (663 nm) in the UV–visible spectra of MB using a JASCO V-570 UV–visible spectrophotometer.

3. Results and discussion

ZnO samples were prepared by simple hydrolysis of zinc acetate with aqueous NaOH in presence of the sodium citrate and PEG as capping/structure directing agents using hydrothermal and sonochemical methods as described in the experimental section. Table 1 illustrates various reaction conditions and detailed reaction parameters for the synthesis of ZnO samples. The as obtained ZnO nanostructures were examined via XRD, FE-SEM, TEM, and different characterization techniques, which are discussed in the following sections.

3.1. XRD analysis

The phase and purity of the as-synthesized samples were investigated by powder X-ray diffraction (XRD) analysis. The typical XRD patterns of all as-synthesized samples obtained by hydrothermal and sonochemical routes are shown in Fig. 1(a) and (b), respectively. It can be seen from the diffraction patterns that, they are nearly identical, regardless of their preparation methods (hydrothermal or sonochemical). All the diffraction peaks can be attributed to crystalline ZnO with hexagonal wurtzite structure. The spectral data are in agreement with JCPDS card no. JCPDS 036-1451 for ZnO [36]. In all the samples, the strong (*hkl*) peaks at 2θ values of 31.79°, 34.42°, 36.25°, 47.51°, 56.62° and 62.83°, corresponding to the lattice planes: (100), (002), (101), (102), (110), and (103), respectively have been observed, indicating lattice constants of a and c equal to 3.25 and 5.21 Å, respectively matching well with ZnO values. No characteristic peaks corresponding to impurities have been observed in the XRD pattern of any sample, which indicates formation of pristine ZnO. The measured intensity ratio, $R_{(002)/(101)}$ of the peaks belonging to (002) and (101) planes for the samples prepared under hydrothermal conditions were found to be 0.86, 0.81, and

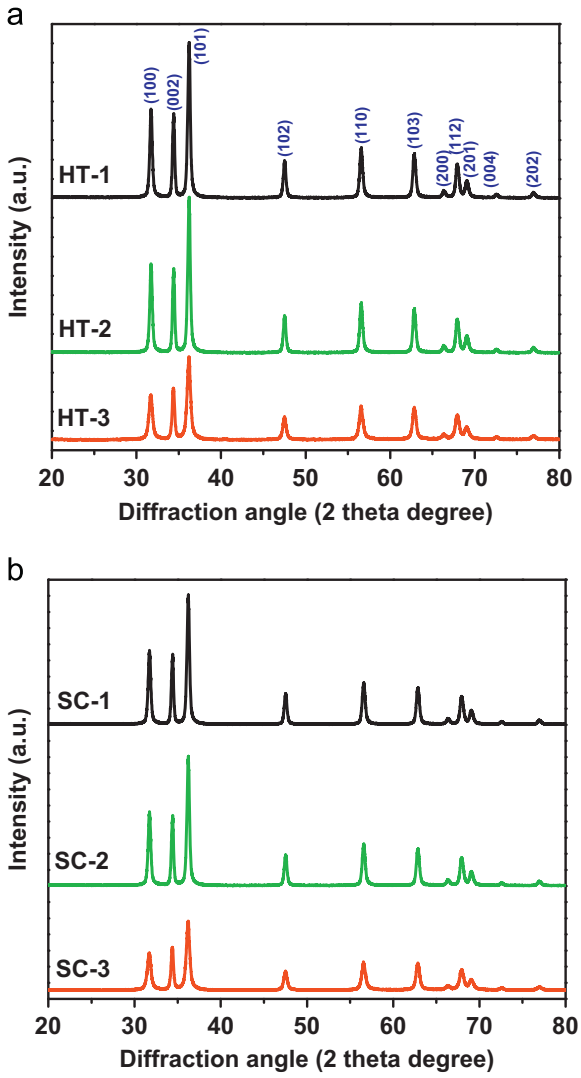

Fig. 1. XRD spectra of ZnO samples prepared under (a) hydrothermal and (b) sonochemical method.

0.79 for HT-1, HT-2, and HT-3 respectively, whereas these values for the samples prepared by the sonochemical method were 0.88, 0.82, and 0.81 for SC-1, SC-2, and SC-3, respectively (Table 1). It could be noted that, in case of all the samples prepared under hydrothermal and sonochemical conditions, the value of $R_{(002)/(101)}$ decreases as the samples are prepared with reduced citrate concentration. Moreover, these values are much higher than the corresponding standard value of 0.44 of bulk hexagonal wurtzite ZnO suggesting (002) orientation of the citrate assisted ZnO samples Similar results were obtained and reported by Raula et al. for ascorbate assisted synthesis of flower-like ZnO nanostructures [37].

3.2. FESEM and TEM characterization

3.2.1. Hydrothermal method

The morphology of the ZnO nanostructures, prepared under different reaction conditions were examined by the FE-SEM technique. Fig. 2 illustrates FE-SEM images of the samples prepared using hydrothermal method. Fig. 2(a)–(c) show the FE-SEM image of the sample HT-1 which reveal the formation of flower-like morphology consisting of stacked tripods composed of uniform sheets with ~150 nm length and 75 nm width. It should be noted that these tripod like structures accumulate and stack on each other to give an overall appearance of flower like morphology. These flower-like nanostructures have been uniformly grown and do not contain any other morphology. However, the size of the nanoflowers was found to vary depending upon the degree of stacking of these nano-tripods. It is worth noting that the morphology of these nanostructures is quite different from those reported earlier, although all of them are termed as flower-like nanostructures. It is known that the concentration of metal ion precursor and the pH of the reaction medium play a crucial role in controlling the shape and size of ZnO nanostructures. To determine the effect of precursor concentration and pH of the reaction media on the formation of typical hierarchical structures, experiments were carried out by systematically lowering the concentration of reactants in the water/PEG mixture. Fig. 2(d) and (e), represents the morphological structures pertaining to sample HT-2 (prepared by using 0.05 M zinc acetate, 0.17 M sodium citrate and 0.9 mM NaOH solutions). Unlike sample HT-1, more pronounced flower-like morphology is developed with well defined petals resembling a *Daheliya* flower like pattern. It can be seen that the ZnO flower comprises of the central thick node adorned with radially arranged petals emerging from the center in a systematic fashion. The size of an individual flower is around 2–3 μm with conical petals of nanometric size. With further lowering of the reactant concentration (viz 0.03 M zinc acetate, 0.11 M sodium citrate and 0.62 mM NaOH aqueous solutions with quantity of PEG and water like that of HT-1 and HT-2) flowerlike morphology was retained however the thick central nodal portion as found in HT-2, opens up fully to evolve a fully bloomed flowers resembling *Jasmine* like morphology (Fig. 2f and g). These flowers show tendency of clinging together. Such transformation from tripod like morphology to the well defined flower like structures can be attributed to the dilution effect of precursors viz. zinc acetate, sodium citrate and NaOH. Thus, it may be concluded that variety of flowerlike ZnO nanostructures can be formed by simply changing the precursor concentrations using hydrothermal route.

More detailed structural information about this flower-like ZnO was obtained from TEM analysis. Fig. 3 shows a selected TEM image and corresponding SAED pattern of a flower-like ZnO nanostructure (sample HT-2). Since TEM provides a two-dimensional projection of a 3D object and hence a star-like pattern is observed in TEM picture. The size of the flower is around 2 μm which matches well with the FE-SEM image. Closer examination of the nanoflowers reveals that the petals are formed from distinct spherical particles. The corresponding SAED pattern (Fig. 3c) indicates the polycrystalline nature of these flowerlike structures.

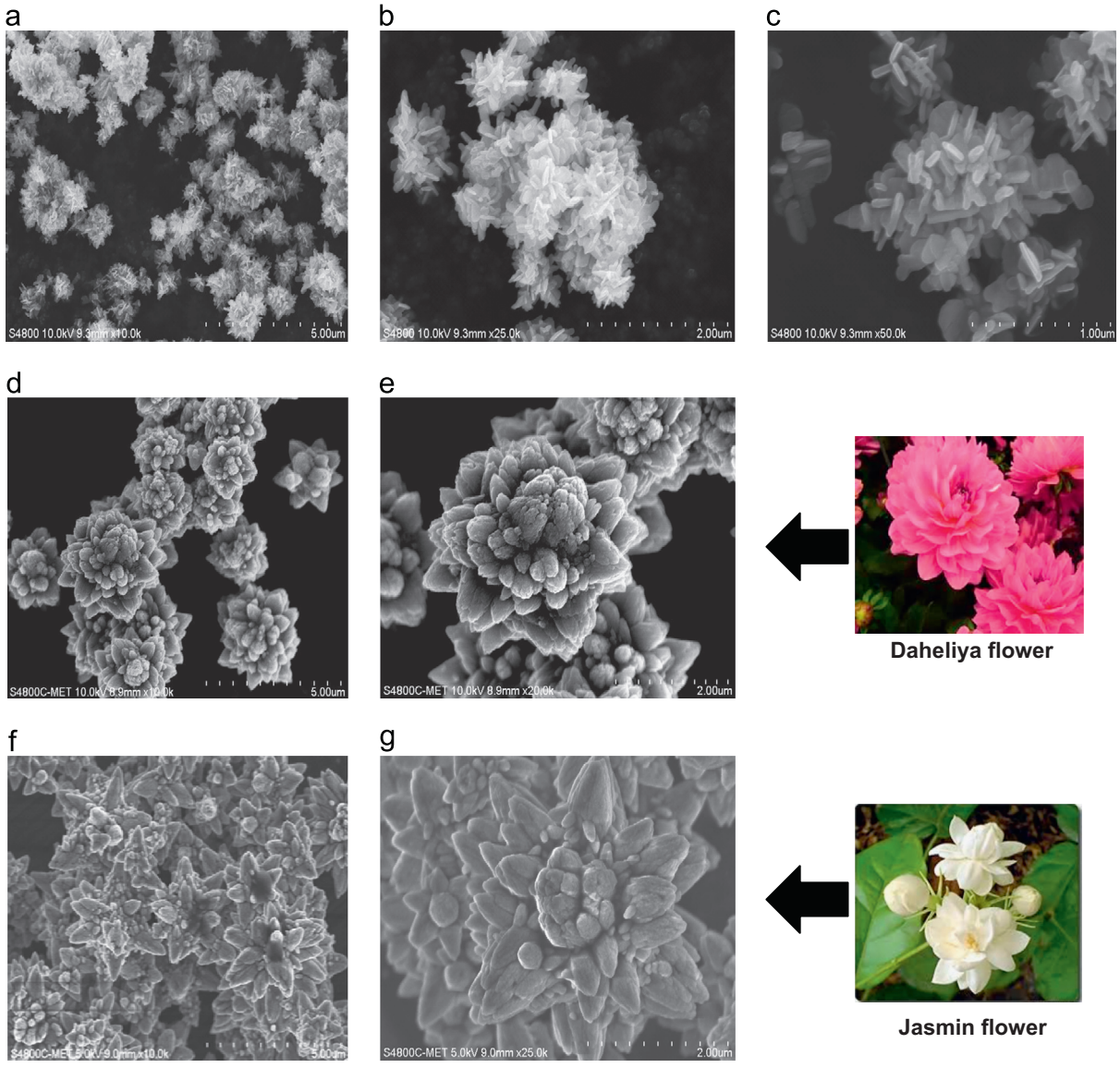

Fig. 2. FE-SEM images of ZnO samples prepared by hydrothermal method: (a–c) HT-1, (d, e) HT-2 and (f, g) HT-3 corresponding to high and low resolutions.

3.2.2. Sonochemical method

In order to study the effect of synthesis method on the morphology of ZnO, experiments with similar precursor concentrations were carried by using sonochemical method. The experimental result revealed that, the synthesis method significantly affects the morphology. An experiment using precursor concentrations of HT-1 (0.1 M zinc acetate, 0.34 M sodium citrate and 1.8 mM NaOH aqueous solutions in PEG with water) under the sonochemical method generates ZnO with cabbage-like morphology. (Sample SC-1). The diameter of the cabbage like structure is found to be around 1.6 μm, which is comprised of randomly assembled nanosheets. (Fig. 4a and b). In case of SC-2 (with 0.05 M zinc acetate, 0.17 M sodium citrate and 0.9 mM NaOH in PEG with water) with lowering precursor concentration, irregularly shaped agglomerated product was obtained (Fig. 4c and d). On further dilution, SC-3 (0.03 M zinc acetate, 0.11 M sodium citrate, 0.62 mM NaOH solutions in PEG in water) the agglomerated product in ellipsoidal shape with diameter around 2 to 5 μm with corrugated surface were obtained (Fig. 4e and f). It seems that the flowerlike morphology might have evolved through these structures by secondary growth via oriented attachment. On the basis of the microscopic data obtained the combined effect of reactant concentration and ultrasound seems to be responsible for evolution of such ellipsoidal ball type morphology which we will discuss in detailed in growth mechanism section.

3.3. Photoluminescence (PL) spectra

Optical properties of ZnO architectures plays important role in their technological applications. The corresponding PL spectra of as-synthesized ZnO nanostructures are

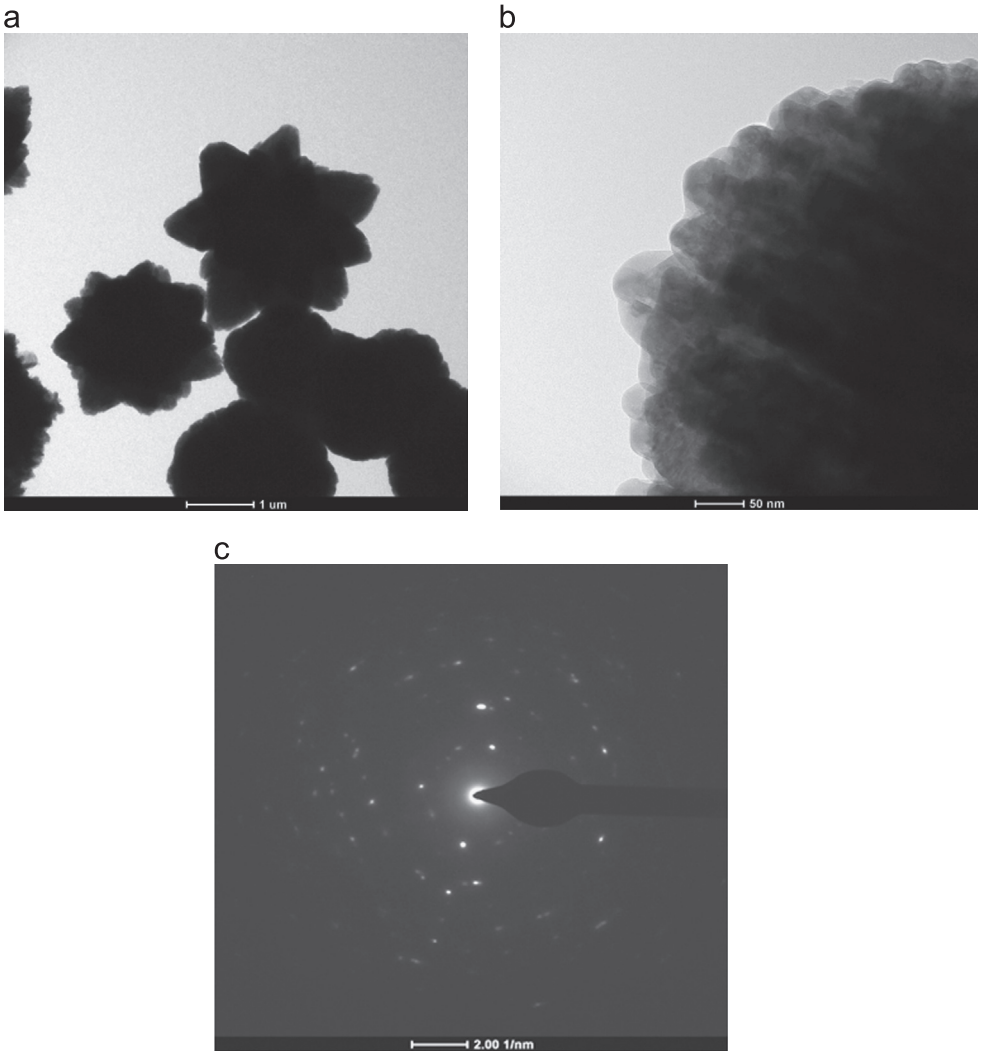

Fig. 3. (a) and (b) TEM images and (c) selected area diffraction (SEAD) pattern of sample HT-2.

shown in Fig. 5. The ZnO PL spectrum is reported to consist of the ultraviolet (UV) emission centered at 381 nm as the near band edge emission and a broad green emission centered at about 510 nm [38]. It is generally accepted that the UV emission of ZnO at 381 nm, corresponding to the recombination of free excitons between conductive band and valence band, which is called near-band-edge emission. It is also suggested that high crystallinity plays a key role in the enhancement of the UV emission. The green-light emission at 510 nm corresponds to the deep level emission. Deep level emissions can have several origins such as single ionized oxygen vacancies, antisite oxygen, donor-acceptor complexes [38–41], and so on. However, in our case only strong a near-band edge UV emission peak at around 380–390 nm is observed for all the synthesized ZnO nanostructures regardless of the preparation methods used, yet the usually observed defect related to deep level emissions were absent, suggesting high optical quality ZnO nanoarchitectures synthesized by both hydrothermal and sonochemical methods. The weak emission peaks observed at 465–470 nm in all the samples can be attributed to the electron transition, mediated by defect levels in the band gap. It is also seen from Fig. 5 that the UV peak intensity of ZnO samples prepared sonochemically is comparatively lower than those of the samples prepared hydrothermally, indicating relatively lower optical quality. As compared with the samples grown by sonochemical method, a slight red shift in UV emission is observed in the hydrothermally grown ZnO samples, which is assumed to be associated with the different compress stress in the ZnO architectures. Thus, the larger compress stress results in narrowing the band gap which further leads to the red shift of near band edge emission.

3.4. FTIR and particle size distribution (PSD) characterization

The FTIR spectrum is an important tool which highlights on the nature of the adsorbed species. FTIR spectra of the representative samples obtained from hydrothermal (HT-1) and sonochemical (SC-1) methods are shown in Fig. 6. The broad band at 3398 cm^{-1} is due to O–H

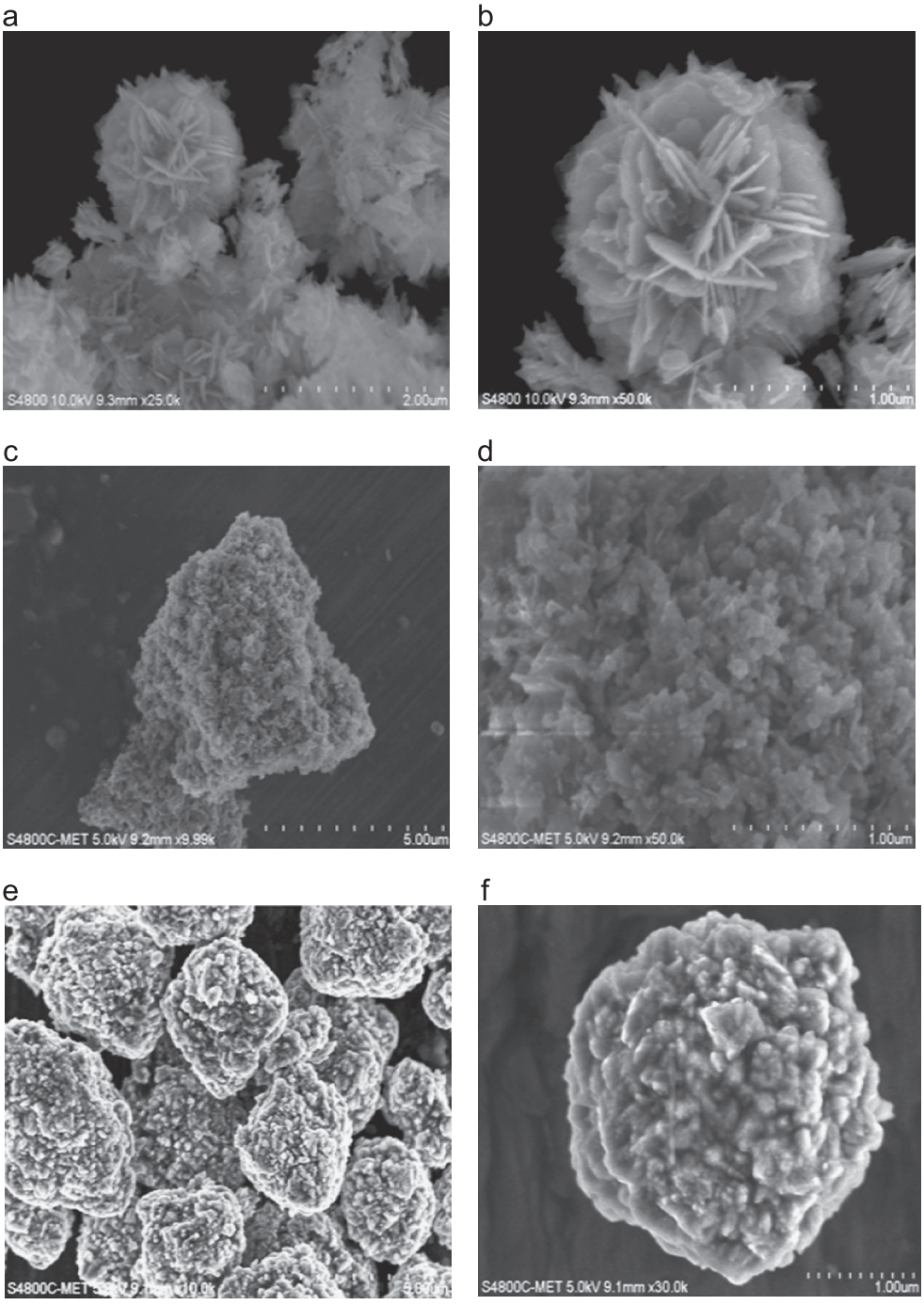

Fig. 4. FE-SEM images of ZnO samples prepared by sonochemical method: (a, b) SC-1, (c, d) SC-2 and (e, f) SC-3 corresponding high resolution images respectively.

stretching vibration of the hydroxyl group. In addition, the peaks observed at 1647 cm^{-1} and 1570 cm^{-1} are due to asymmetric and symmetric stretching modes of carboxylate ions respectively. The peaks observed at 902 cm^{-1} and 543 cm^{-1} can be assigned to C–C stretching mode and M–O stretching vibrations respectively. These results clearly indicate the adsorption of carboxylate ions on the surface of the ZnO nanostructures.

Fig. 7 discloses the particle size distribution histogram of zinc oxide nanostructures synthesized using hydrothermal and sonochemical methods. A comparison of the results indicates that, independent of the preparation method, the particle size decreases with reduction in the reactants' concentration. The mean diameters for the hydrothermally prepared samples viz. HT-1, HT-2 and HT-3 were found to be 98, 88 and 58 nm, respectively. Similarly, for sonochemically prepared samples viz. SC-1, SC-2 and SC-3 the values are 218, 170 and 122 nm, respectively. These results can be correlated to the concentration of reactants with respect to amount of PEG used. It is believed that, the

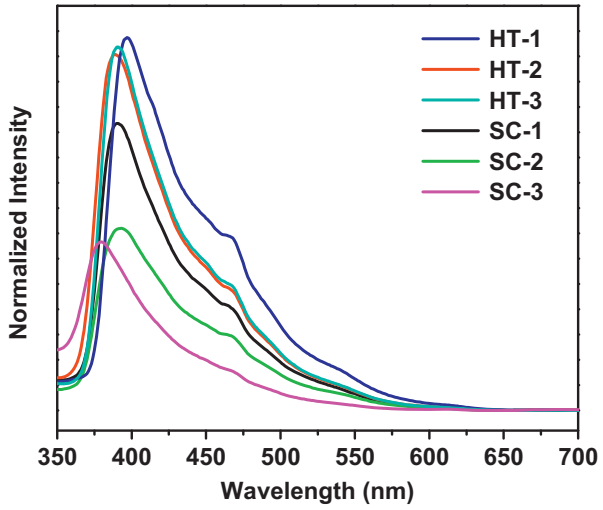

Fig. 5. Photoluminescence (PL) spectra of different ZnO samples prepared by hydrothermal and sonochemical methods.

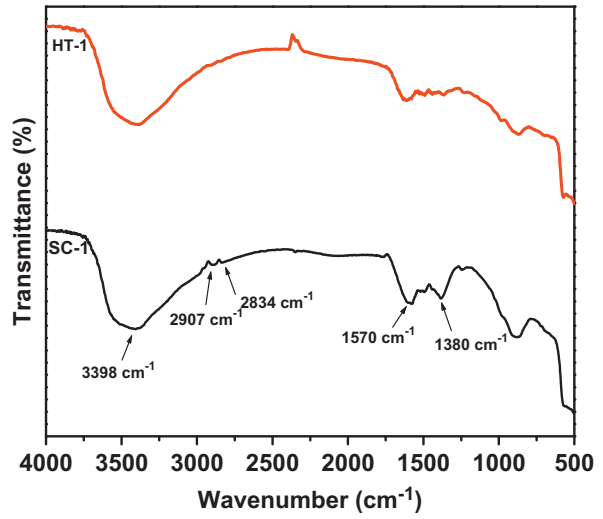

Fig. 6. FTIR spectrum of representative ZnO samples; HT-1, and SC-1.

PEG plays a protective role in which linear flexible molecules can easily adsorb surface of oxides. Such adsorbed layer provides a good steric protection against aggregation [42,43]. Thus, the concentration of reactants with respect to quantity of PEG plays an important role in building-up of the typical architectures.

3.5. Plausible growth mechanism

On the basis of the morphologies obtained, a probable growth mechanism for the formation of different hierarchal ZnO nanostructures is proposed in Fig. 8. ZnO exhibits a hexagonal wurtzite structure consisting of planes of tetrahederally coordinated O^{2-} and Zn^{2+} ions, mounted alternately along the polar *c*-axis. The well developed crystal faces of ZnO evince positively charged polar (0001)-Zn surfaces, six symmetric nonpolar $(1\bar{0}10)$ planes of the side facets and negatively charged $(00\bar{0}1)$-O polar surfaces [44]. The crystal growth rate in different directions generally follows the order $[0001] > [1\bar{0}10] \geq [1\bar{0}\bar{1}1] > [1\bar{0}11] > [00\bar{0}1]$ [45]. During the course of reaction, zinc acetate produces Zn^{2+} cation which readily reacts with OH^- anions forming the basic growth unit $[Zn(OH)_4]^{2-}$. These $[Zn(OH)_4]^{2-}$ ions then decompose to generate ZnO molecular species [37].

$$Zn^{2+} + 4OH^- \rightarrow [Zn(OH)_4]^{2-} \quad (1)$$

$$[Zn(OH)_4]^{2-} \rightarrow ZnO + H_2O + 2OH^- \quad (2)$$

Cheon et al. have reported that there are four different parameters, kinetic energy barrier, temperature, time and capping molecules that can influence the growth pattern of nanocrystals under nonequillibrium kinetic growth conditions in the solution based approach [46]. For the formation of flower type ZnO architecture consisting of stacked tripod, it seems that as the reaction proceeds, the surfaces whose normal directions are of fast growth rate disappear while the slow growing surfaces remain. We believe, in our synthetic architecture, during citrate and PEG assisted hydrothermal and sonochemical synthesis, the capping agents, citrate and PEG plays an important role for the formation of these hierarchical nanostructures (Figs. 2(a and b) and 3(a and b)). During the citrate assisted process, large quantity of negatively charged $[Zn(C_6H_5O_7)_4^{-12}]^{-10}$ complex ions are in existence. These negatively charged ions along with PEG are preferably adsorbed on the positive polar plane {0001} by competing with growth units, which minimizes the anisotropic growth of ZnO along {0001} direction. However, there exist inevitable defects or bulges on the lateral planes of the initially formed ZnO crystals. Such bulges will preferentially grow along the $(0\bar{1}10)$ direction with lagging {0001} direction within the $(\bar{2}\bar{1}10)$ plane resulting into formation of vertically standing nanosheets on the lateral surface [47]. Moreover, there also exist some outshoots on the growing nanosheets. These outshoots will grow and lead to the formation of secondary branched nanosheets with terminated $(\bar{2}\bar{1}10)$ facets and interplaner angles 60°. As the hydrothermal reaction time proceeds, third or fourth branched nanosheets could be formed on the as-grown nanosheets resulting into formation of flower having stacked tripod-like ZnO architecture.

While in case of sonochemical environment, more and more nanosheets with $(\bar{2}\bar{1}10)$ planer surface interlaced and overlapped with each other into a multilayered network structure resulting in to the hierarchical ZnO cabbage-like microstructure. The overall mechanism is schematically presented in Fig. 8. Further, in a very early stage, as the dehydration reaction (Eq. (2) above) progresses, more and more ZnO clusters are formed in the solution. Subsequently, the nucleation starts and thermodynamically stable (lower surface energy) spherical/quasi-spherical ZnO seeds (~20–30 nm) starts to form in the solution as mentioned elsewhere [46,48]. Also, in nucleation stage, the growth of ZnO nanostructures largely depends on the concentration of the reactants irrespective of the presence of any foreign

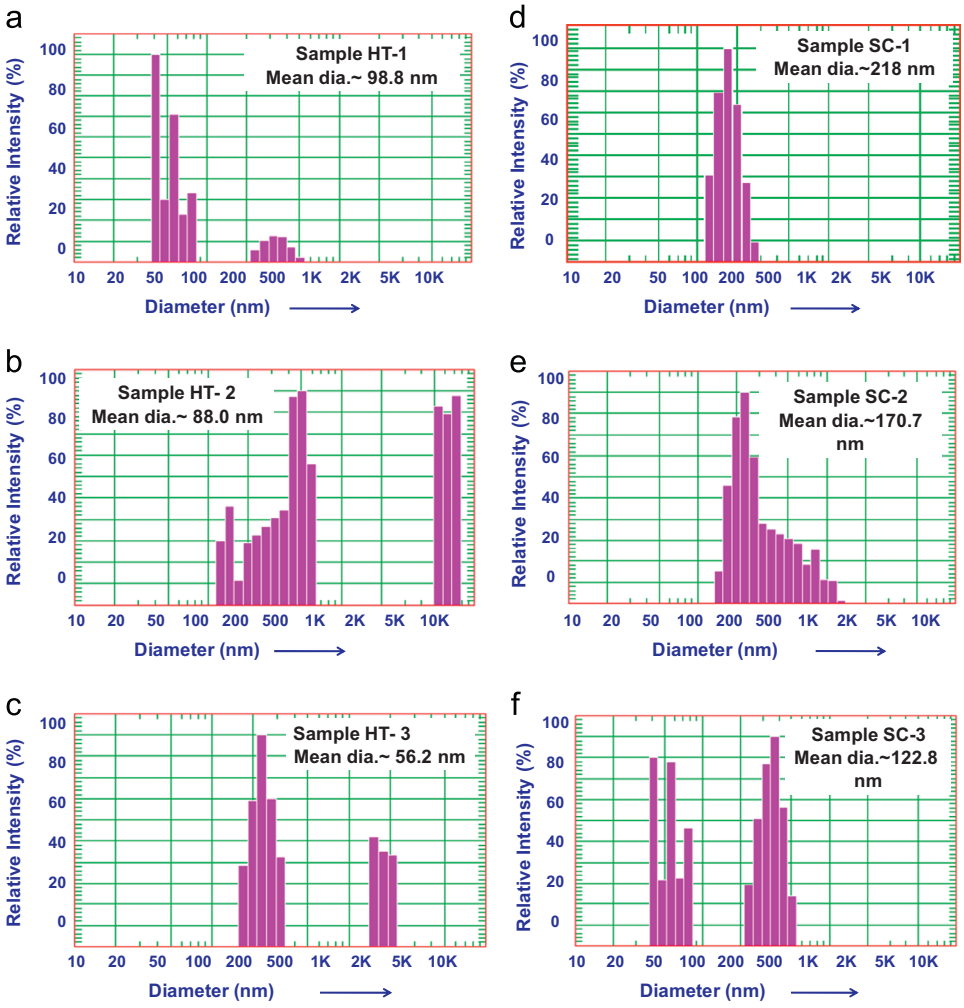

Fig. 7. Particle size distribution histograms of different ZnO architectures.

agent such as surfactant, polymer, or other additives in the reaction medium. However, at the time of secondary growth process, the additives (structure directing agents) are adsorbed onto preferred planes and alter growth kinetics. In our case, for the flowerlike morphology of samples HT-2 and HT-3, we tend to suggest that the concentration of the reactants used was responsible for the formation of thermodynamically stable product. We believe that, this flowerlike morphology arises from oriented attachment of the initially formed spherical/quasi-spherical/ellipsoidal ZnO nanocrystallites in a particular plane. Formation of such primary crystallites in our case is evident from the FESEM images of sample ZnO/HT-2 (Fig. 2c–f), which were prepared at reduced reactant concentration.

It is well known that for kinetically controlled products, the flux of reactants largely determine the shape of the particles formed [49]. As reported by Peng et al. [49], with the increase in the flux of reactant concentration, gradual evolution of shape occurs through zero dimensions to one dimension and so on to three dimensions [50]. Moreover, it is evident that the relatively higher ultrasonic frequency is also helpful for the preparation of hierarchical ZnO structures. At higher concentrations of the reactants, the alteration of expansion and compression of the local liquids is slower and longer periods are left for negative pressure resulting into less frequent collapse of bubbles and thus the effect of shock waves and microjets may not displayed adequately. The reaction system under this condition is similar to that without exertion of ultrasonic irradiation and leads to thermodynamically stable product; as a result, ZnO prepared with relatively higher reactant concentration (sample SC-1) possesses cabbage-like morphology. At still reduced reactant concentrations (Sample SC-2 and SC-3), collapse of bubbles was capable of producing shock waves and microjets that bombarded and eroded the primary ZnO crystallites more frequently. In this case, the secondary growth was effectively inhibited/suppressed and as a result of this agglomerated product with irregular shape and ellipsoidal balls with corrugated surface was formed in case of samples SC-2 and SC-3 respectively. (Fig. 4c–f).

3.6. Photocatalytic activity

The use of ZnO for the photocatalytic degradation of organic pollutants in aqueous solution is well established. To demonstrate the potential applicability of our ZnO samples, the photocatalytic degradation of methylene blue (MB) was

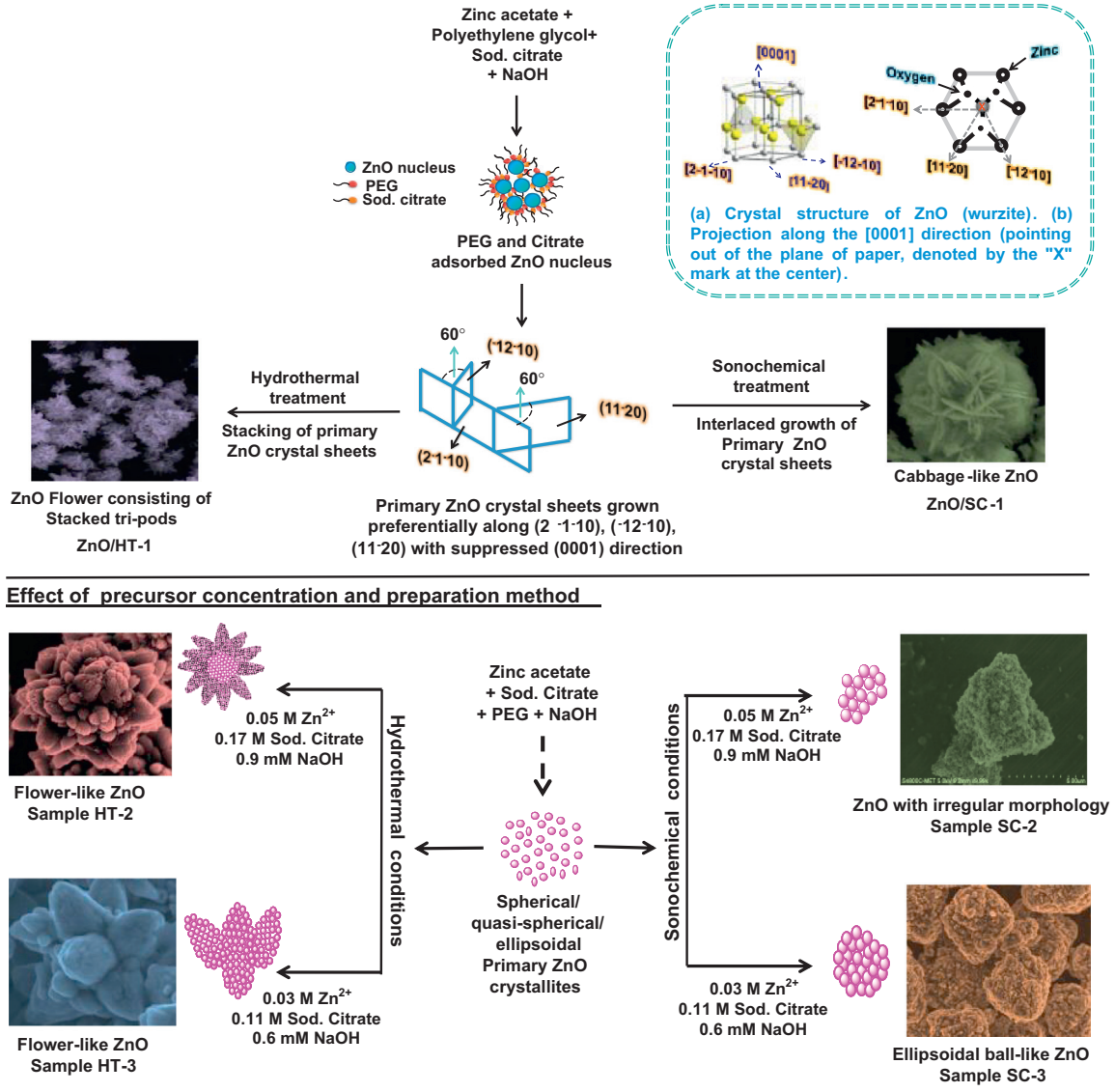

Fig. 8. Schematic presentation of the formation of different hierarchical ZnO samples prepared by hydrothermal and sonochemical methods with different precursor concentrations.

chosen as a reference, and the characteristic absorption of MB appearing at 663 nm was selected for monitoring photocatalytic degradation process. The absorption spectra of aqueous solution of MB (100 ppm, 100 mL) in presence of 50 mg of ZnO flower-like structure (HT-2) under sunlight for different time interval is shown in Fig. 9(a). The absorption peak corresponding to MB at 663 nm reduces by 50% within 15 min and completely disappears after irradiation for ~60 min. Further experiments were carried out by using other as-synthesized ZnO samples under similar conditions to evaluate the morphology induced performance towards photocatalytic degradation of MB. Fig. 9(b) shows variation in the concentration of MB with sunlight irradiation time over the as-prepared ZnO samples. A blank experiment, without any catalyst was also performed. It does not show any significant reduction in the concentration of MB under sunlight irradiation. However, addition of ZnO catalysts leads to the degradation of MB, and it is also observed that the photocatalytic activity depends on the morphology of the ZnO. The photocatalytic activity increases in turn for the ZnO catalysts: ZnO/SC-3, ZnO/SC-1, ZnO/SC-2, ZnO/HT-3, ZnO/HT-1 and ZnO/HT-2. Herein, the ZnO/HT-2 sample exhibits highest photocatalytic activity, of around 96% within 60 min irradiation. Kim et al. [51] have reported that the maximum degradation of Methylene blue under UV-light (1 kW) irradiation by 1.5 g/L rod- and spherical-shaped ZnO nanoparticles was 98.5% and 74%, respectively. Compared to their findings, our flower-like ZnO/HT-2 catalyst demonstrates advantage of being active at the lower catalyst concentration and under sunlight irradiation, indicating a facile and cost effective degradation by the hierarchically grown ZnO structures. It is well known that the surface area of catalyst contributes in the photocatalytic activities. However, there are reports in the literature demonstrating the low photocatalytic performances of hierarchical ZnO structures even with higher

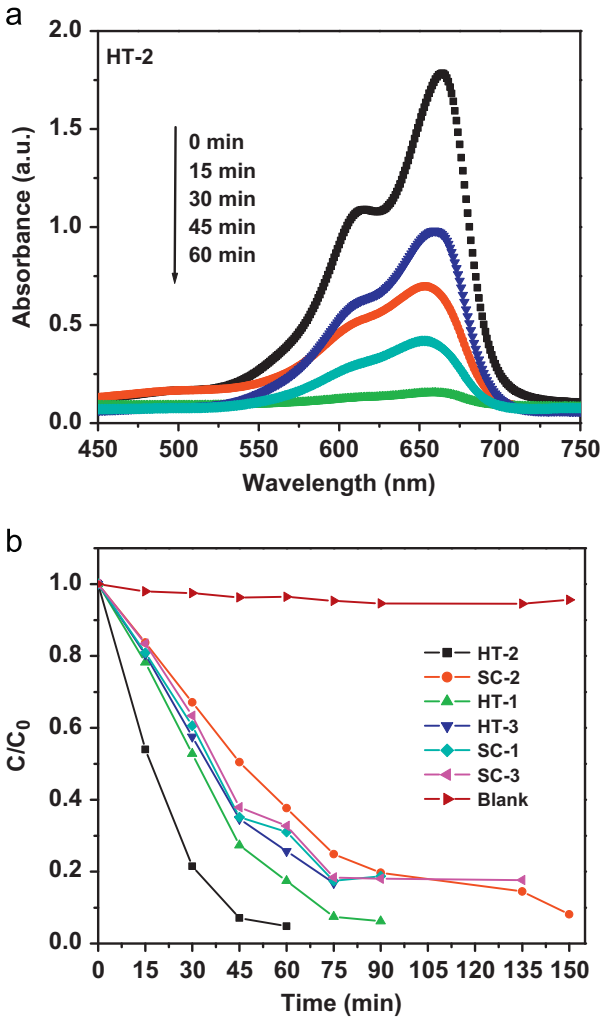

Fig. 9. (a) Time dependent optical absorption spectra for Methylene blue (MB) in presence of flowerlike ZnO (sample HT-2) under sunlight irradiation and (b) MB concentration changes over photocatalyst-free solution, and other hierarchical ZnO nanostructures. (Initial concentration: 100 ppm, 100 mL; catalyst dose: 50 mg).

surface areas [52,53]. In our case, high crystallinity and the specific crystal face ($I_{(002)/(101)}$): Table 1) might be contributing towards the enhancement in the photocatalytic activity. The possible account for flower-shaped samples with enhancement in photocatalytic activity can be attributed to more exposure of polar faces which bind S and N atoms of the methylene blue ($C_{16}H_{18}N_3SCl$) molecules and then photocatalyze it. Further investigations on the factors accounting for different photoactivities are in progress.

4. Conclusion

In conclusion, the present study outlines facile hydrothermal and sonochemical routes to synthesize hierarchical ZnO architectures with improved photocatalytic activity. The morphologies of obtained samples could be controlled by adjusting the precursor concentrations and the synthesis method. It is observed that precursor concentration and the preparation method have significant effect on the morphology of the final product. Accordingly, flower-like, cabbage-like, ellipsoidal ball-like ZnO architectures can be obtained. Flower-like ZnO (HT-2) exhibits excellent photocatalytic activity for degradation of MB dye. The as-synthesized ZnO hierarchical structures are also expected to be useful for other applications such as gas sensing and organic transformations. Moreover, this work further hints that such facile, green and economic approach can be applied to synthesize other metal-oxides with novel morphologies.

Acknowledgments

I.S. Mulla gratefully acknowledges CSIR, New Delhi, India for awarding him the Emeritus Scientist Scheme.

References

[1] M.H. Huang, S. Mao, H. Feick, H. Yan, Y. Wu, H. Kind, E. Weber, R. Russo, P. Yang, Room-temperature ultraviolet nanowire nanolasers, Science 292 (2001) 1897–1899.
[2] L. Vayssieres, K. Keis, A. Hagfeldt, S.E. Lindquist, Three-dimensional array of highly oriented crystalline ZnO microtubes, Chemistry of Materials 13 (2001) 4395–4398.
[3] R. Konenkamp, L. Dloczik, K. Ernst, C. Olecsh, Nano-structures for solar cells with extremely thin absorbers, Physica E 14 (2002) 219–223.
[4] D.M. Bagnall, Y.F. Chen, Z. Zhu, T. Yao, S. Koyama, M.Y. Shen, T. Goto, Optically pumped lasing of ZnO at room temperature, Applied Physics Letters 70 (1997) 2230–2232.
[5] H. Cao, J.Y. Xu, D.Z. Zhang, S.H. Chang, S.T. Ho, E.W. Seelig, X. Liu, R.P.H. Chang, Spatial confinement of laser light in active random media, Physical Review Letters 84 (2000) 5584–5587.
[6] X.F. Duan, Y. Huang, R. Agarwal, C.M. Lieber, Single-nanowire electrically driven lasers, Nature 421 (2003) 241–244.
[7] Q. Wan, Q.H. Li, Y.J. Chen, T.H. Wang, X.L. He, J.P. Li, C.L. Lin, Fabrication and ethanol sensing characteristics of ZnO nanowire gas sensors, Applied Physics Letters 84 (2004) 3654–3656.
[8] Y. Darici, P.H. Holloway, J. Sebastian, T. Trottier, S. Jones, J.J. Rodriquez, Electron beam dissociation of CO and CO_2 on ZnS thin films, Vacuum Science & Technology 17 (1999) 692–697.
[9] Y. Lu, I.A. Dajani, R.J. Knize, ZnO nanorod arrays as p–n heterojunction ultraviolet photodetectors, Electronics Letters 42 (2006) 1309–1310.
[10] M. Law, L. Greene, J.C. Jonhnson, R. Saykally, P. Yang, Nanowire dye-sensitized solar cells, Nature Materials 4 (2005) 455–459.
[11] Y. Cui, Z. Zhong, D. Wang, W.U. Wang, C.M. Lieber, High performance silicon nanowire field effect transistors, Nano Letters 3 (2003) 149–152.
[12] B.S. Kang, F. Ren, Y.W. Heo, L.C. Tien, D.P. Norton, S.J. Pearton, pH measure,emts with single ZnO nanorods integrated with microchannels, Applied Physics Letters 86 (2005) 112105–112105.
[13] K. Tominaga, N. Umezu, I. Mori, T. Ushiro, T. Moriga, I. Nakabayashi, Transparent conductive ZnO film preparation by alternating sputtering of ZnO:Al and Zn or Al targets, Thin Solid Films 334 (1998) 35–39.
[14] T. Minami, S. Ida, T. Miyata, Y. Minamino, Transparent conducting ZnO thin films deposited by vacuum arc plasma evaporation, Thin Solid Films 445 (2003) 268–273.
[15] Z.L. Wang, Nanostructures of zinc oxide, Mater. Today 7 (2004) 26–33.
[16] B. Xiang, P. Wang, X. Zhang, S.A. Dayeh, D.P.R. Aplin, C. Soci, D. Yu, D. Wang, Rational synthesis of p-type zinc oxide nanowire

arrays using simple chemical vapor deposition, Nano Letters 7 (2007) 323–328.
[17] C. Geng, Y. Jiang, Y. Yao, X. Meng, J.A. Zapien, C.S. Lee, Y. Lifshitz, S.T. Lee, Well-aligned ZnO nanowire arrays fabricated on silicon substrates, Advanced Functional Materials 14 (2004) 589–594.
[18] C.S. Lao, P.X. Gao, R.S. Yang, Y. Zhang, Y. Dai, Z.L. Wang, Formation of double-side teethed nanocombs of ZnO and self-catalysis of Zn-terminated polar surface, Chemical Physics Letters 417 (2006) 358–362.
[19] Z.W. Pan, Z.R. Dai, Z.L. Wang, Nanobelts of semiconducting oxides, Science 291 (2001) 1947–1949.
[20] X.Y. Kong, Y. Ding, R. Yang, Z.L. Wang, Single-crystal nanorings formed by epitaxial self-coiling of polar nanobelts, Science 303 (2004) 1348–1351.
[21] J. He, Y.H. Huang, Y. Zhang, Y.S. Gu, Z. Ji, C. Zhou, Large-scale synthesis, microstructure and growth mechanism of self-assembled core–shell ZnO/SiO_x nanowires, Materials Letters 60 (2006) 150–153.
[22] Y. Feng, M. Zhang, M. Guo, X. Wang, Studies on the PEG-assisted hydrothermal synthesis and growth mechanism of ZnO microrod and mesoporous microsphere arrays on the substrate, Crystal Growth & Design 10 (2010) 1500–1507.
[23] H. Zhang, D. Yang, D. Li, X. Ma, S. Li, D. Que, Controllable growth of ZnO microcrystals by a capping-molecule-assisted hydrothermal process, Crystal Growth & Design 5 (2005) 547–550.
[24] J. Yin, Q. Lu, Z. Yu, J. Wang, H. Pang, F. Gao, Hierarchical ZnO nanorod-assembled hollow superstructures for catalytic and photoluminescence applications, Crystal Growth & Design 10 (2010) 40–43.
[25] Q. Wu, X. Chen, P. Zhang, Y. Han, X. Chen, Y. Yan, S. Li, Amino acid-assisted synthesis of ZnO hierarchical architectures and their novel photocatalytic activities, Crystal Growth & Design 8 (2008) 3010–3018.
[26] P. Mishra, R.S. Yadav, A.C. Pandey, Growth mechanism and photoluminescence property of flower-like ZnO nanostructures synthesized by starch-assisted sonochemical method, Ultrasonics Sonochemistry 17 (2010) 560–565.
[27] U. Pal, P. Santiago, Controlling the morphology of ZnO nanostructures in a low-temperature hydrothermal process, Journal of Physical Chemistry B 109 (2005) 15317–15321.
[28] A. Taubert, G. Glasser, D. Palms, Kinetics and particle formation mechanism of zinc oxide particles in polymer-controlled precipitation from aqueous solution, Langmuir 18 (2002) 4488–4494.
[29] J. Du, Z. Liu, Y. Huang, Y. Gao, B. Han, W. Li, G. Yang, Control of ZnO morphologies via surfactants assisted route in the subcritical water, Journal of Crystal Growth 280 (2005) 126–134.
[30] M.V. Vaishampayan, I.S. Mulla, S.S. Joshi, Optical and photocatalytic properties of single crystalline ZnO at the air–liquid Interface by an aminolytic reaction, Langmuir 20 (2011) 12751–12759.
[31] J. Duan, X. Huang, E. Wang, EG-assisted synthesis of ZnO nanotubes, Materials Letters 60 (2006) 1918–1921.
[32] T. Thongtem, S. Jattukul, A. Phuruangrat, S. Thongtem, The effect of H_2O and PEG on the morphologies of ZnO nanostructures synthesized under microwave radiation, Journal of Alloys and Compounds 491 (2010) 654–657.
[33] Z. Zhu, D. Yang, H. Liu, Microwave-assisted hydrothermal synthesis of ZnO rod-assembled microspheres and their photocatalytic performances, Advanced Powder Technology 22 (2011) 493–497.
[34] H. Zhang, D. Yang, X. Ma, N. Du, J. Wu, D. Que, Straight and thin ZnO nanorods: hectogram-scale synthesis at low temperature and cathodoluminescence, Journal of Physical Chemistry B 110 (2006) 827–830.
[35] Y. Zeng, T. Zhang, W. Fu, Q. Yu, G. Wang, Y. Zhang, Y. Sui, L. Wang, C. Shao, Y. Liu, H. Yang, G. Zou, Fabrication and optical properties of large-scale nutlike ZnO microcrystals via a low-temperature hydrothermal route, Journal of Physical Chemistry C 113 (2009) 8016–8022.
[36] American Society for Testing and Material, Powder Diffraction Files, Joint Committee on Powder Diffraction Standards, Swartmore, PA (1999) 3–888.
[37] M. Raula, M.H. Rashid, T.K. Paria, E.T. Dinda, K. Mandal, Ascorbate-assisted growth of hierarchical ZnO nanostructures: sphere, spindle, and flower and their catalytic properties, Langmuir 26 (2010) 8769–8782.
[38] K. Vanheusden, W.L. Warren, C.H. Seager, Mechanisms behind green photoluminescence in ZnO phosphor powders, Journal of Applied Physics 79 (1996) 7983–7990.
[39] B. Lin, Z. Fu, Y. Jia, Green luminescent center in undoped zinc oxide films deposited on silicon substrates, Applied Physics Letters 79 (2001) 943–945.
[40] S.A. Studenikin, M. Cocivera, Time-resolved luminescence and photoconductivity of polycrystalline ZnO films, Journal of Applied Physics 91 (2002) 5060–5065.
[41] D.C. Reynolds, D.C. Look, B. Jogai, Fine structure on the green band in ZnO, Journal of Applied Physics 89 (2001) 6189–6191.
[42] E. Dickson, L. Eriksson, Particle flocculation by adsorbing polymers, Advances in Colloid and Interface Science 34 (1991) 1–29.
[43] S. Quintillan, C. Tojo, M.C. Blanco, M.A. López-Quintela, Effects of the intermicellar exchange on the size controll of nanoparticles in microemulsions, Langmuir 17 (2001) 7251–7254.
[44] S. Komarneni, M. Bruno, E. Mariani, Synthesis of ZnO with and without microwaves, Materials Research Bulletin 35 (2000) 1843–1847.
[45] A. Wei, X.W. Sun, C.X. Xu, Z.L. Dong, Y. Yag, S.T. Tan, W. Huang, Growth mechanism of tubular ZnO formed in aqueous solution, Nanotechnology 17 (2006) 1740–1744.
[46] S.M. Lee, S.N. Cho, J. Cheon, Anisotropic shape control of colloidal inorganic nanocrystals, Advanced Materials 15 (2003) 441–444.
[47] F. Lu, W. Cai, Y. Zhang, ZnO hierarchical micro/nanoarchitectures: solvothermal synthesis and structurally enhanced photocatalytic performance, Advanced Functional Materials 18 (2008) 1047–1056.
[48] Y.W. Jun, J.S. Choi, J. Cheon, Shape control of semiconductor and metal oxide nanocrystals through nonhydrolytic colloidal routes, Angewandte Chemie International Edition 45 (2006) 3414–3439.
[49] Z.A. Peng, X. Peng, Mechanisms of the shape evolution of CdSe nanocrystals, Journal of the American Chemical Society 123 (2001) 1389–1395.
[50] B.D. Yao, Y.F. Chan, N. Wang, Formation of ZnO nanostructures by a simple way of thermal evaporation, Applied Physics Letters 81 (2002) 757–759.
[51] S.J. Kim, D.W. Park, Preparation of ZnO nanopowders by thermal plasma and characterization of photo-catalytic property, Applied Surface Science 255 (2009) 5363–5367.
[52] X. Wang, Q. Zhang, Q. Wan, G. Dai, C. Zhou, B. Zhou, Controllable ZnO architectures by ethanolamine-assisted hydrothermal reaction for enhanced photocatalytic activity, Journal of Physical Chemistry C 115 (2011) 2769–2775.
[53] L. Sun, R. Shao, Z. Chen, L. Tang, Y.J. Ding, Alkali-dependent synthesis of flower-like ZnO structures with enhanced photocatalytic activity via a facile hydrothermal method, Applied Surface Science 258 (2012) 5455–5461.